Quantifying the average potential state of the canopy using the bioclimatic optimality hypothesis

A.I. Ciobanas [a,*],

[a] *INRS-ETE, 490, rue de la Couronne, Quebec (Qc), G1K 9A9, CANADA*

A.N. Rousseau [b]

[b] *INRS-ETE, 490, rue de la Couronne, Quebec (Qc), G1K 9A9, CANADA*

Abstract

Following the approach developed by Eagleson (2002), we analyzed the optimal state of vegetation given the influence of the three major plant stresses: heat, light and water availability. The analysis of plants under heat and light constraints showed that, given potential conditions (unlimited access to water of Eagleson), the optimal vegetation state can be defined by two conditions (the heat and the light propositions). We also evidenced the crucial role played by stomatal regulation on the thermal state and water balance of the leaf. As well, we showed that plants have great interest in adapting their water transport capacity to the local transpiration demand. To test the hypothesis relative to the heat proposition, we modeled the thermal state of the vegetation cover. For 32 FLUXNET sites around the globe, we investigated the variation of the vegetation thermal state with respect to the stomatal resistance r_s. We showed that plants can significantly thermoregulate their temperature by means of the stomatal resistance and that there is a critical stomatal resistance, $\overline{r}_s^T$, corresponding to a thermal state of plant such that the air and the vegetation temperature are equal when averaged over the growing season. We showed that, for sites characterized by highly evolved plants, this optimal thermal state defined by $\overline{r}_s^T$ is indeed selected by plants when potential conditions are met. In this light, $\overline{r}_s^T$ becomes an important parameter defining the potential state of plants, easily computed for any sites around the world.

Key words: optimal bioclimate, evapotranspiration, Fluxnet network

* Corresponding author.
Email addresses: Alexandru.Ciobanas@ete.inrs.ca (A.I. Ciobanas), Alain.Rousseau@ete.inrs.ca (A.N. Rousseau).

1 Introduction

It is well known that the evapotranspiration (ET) phenomenon strongly influences all hydrological processes at various length scales. In fact, in arid and humid regions ET plays a central role within the hydrological cycle since 100% to 60% of the total precipitation input to a watershed goes back to the atmosphere (Hall (1971); Brutsaert (2005)). In this context, a correct estimation of actual ET (AET) is of great importance for various fields like agronomy, meteorology and climatology. Unfortunately, reliable estimates of AET are difficult to make since the AET is a direct consequence of the complex interactions between the soil, the plants and the atmosphere. One of the most recognized, physically-based model of ET is the Penman-Monteith (PM) model (Monteith (1965); Rijtema (1965)). This model relies entirely on the physics of evaporation at the ground surface and takes into account the three driving forces of evaporation: the supply of energy, the supply of water and, finally, the water vapor and heat transport capacity of the atmosphere above the ground. Given the surface resistance to evaporation, r_s and the aerodynamic transfer coefficients, the PM model can be used to estimate AET. While aerodynamic transfer coefficients can be quite easily estimated by characterizing the turbulent surface boundary layer, the modeling of r_s is far more complex. That is because r_s is highly dependent on plant physiology which in turn reacts to many external constraints like temperature, water availability in the soil and level of insolation. In a need to simplify this intricate problem, researchers have tried to express AET with respect to a potential ET (PET):

$$AET = k_p PET \tag{1}$$

where PET is defined as the ET from vegetation or soil system obtained when the supply of water to the soil is abundant (Peart and Curry (1998)) and k_p is a constant multiplier (< 1) also known as the crop coefficient, which mainly depends on climate, vegetation type, and soil dryness. Hence, the concept of PET simplifies the problem by fixing one of the important parameters of the soil and vegetation: the level of water supply to the plant root system. To compute the PET, the PM model uses the concept of reference evapotranspiration by simply computing the ET rate using a set of fixed parameters corresponding to a well defined reference crop (Allen et al. (1994a,b)). Due to its sound physical basis and incorporation of plant physiological and aerodynamic parameters the PM model, coupled with the concept of reference crop, has been recommended as the primary method for the computation of PET . However, due to the large structural differences between canopy types (forests, grasslands, tundra, etc) the use of a reference crop for estimating the PET can be unrealistic. This calls for a constant calibration of k_p with respect to the vegetation type and local climate.

More recently Shuttleworth (2006) introduced the so-called "one-step approach" for the computation of AET. He points out that, instead of computing PET with the PM model and then correcting it using the crop coefficient, one should directly compute AET using the PM model with a characteristic surface resistance, $\overline{r}_s$, corresponding to the *average evaporative state* of the vegetation crop over a longer period of time. The time scale of this average state is of the order of the growing season. The main difficulty in using this approach is the absence of all-day average surface resistances for different crops (Farahani et al. (2007)). This shortcoming was partially overcame by transforming the already available crop coefficients for different biomes into characteristic $\overline{r}_s$ (Shuttleworth (2006)).

Hence, the main difficulty in using PM model is the absence of a reliable model for the average surface resistance which would correspond to the potential state of vegetation. Of course the definition of such a parameter can make sense only if plants chose a particular potential state when water is not a limiting factor for them. One interesting starting point for solving this problem can be constituted by Eagleson (2002) recent work which analyzed the optimal state of vegetation given the influence of the three major plant stresses: the heat, the light and the water availability. Under the assumption that plants prefer a zero-stress average state, Eagleson (2002) derived the necessary relations among species, soil and local climate such that the plant productivity is maximized. These relations quantify the optimal state of the plant and are called *the heat, the light and the water propositions*.

The main aim of this study is to analyze in more detail the strong influence of heat and light on plant productivity in order to identify some important mechanisms by which plants can adapt to these environmental constraints. By analyzing first the influence of the leaf temperature on plant productivity, we evidence the importance of stomatal modulation for the thermal regulation of the leaf. We also identify that there is a critical surface resistance $\overline{r}_s^T$ which precisely corresponds to the optimal thermal state of plants as defined by the heat proposition. By analyzing then the plant light response we showed that, in order to function optimally, plants need to adapt their water transport capacity to the local insolation constraint I_0. Finally, we implement an energy balance model of the vegetation canopy in order to investigate the influence of the surface resistance on the thermal state of plants. Using the FLUXNET meteorological and surface fluxes data set (Baldocchi et al. (2001)) we quantitatively demonstrate that, given potential conditions, evolved plants prefer a thermal state characterized by a quasi-isothermal evaporation process, in accordance with Eagleson's heat proposition.

2 Model

To quantify the thermal state of the vegetation one has to solve the energy balance at the leaves surface in order to find the leaf temperature and consequently the surface fluxes (the latent and sensible heat fluxes). The approximate energy balance at the leaf surface is:

$$R_n = L_e E + H \quad \left[W/m^2\right] \tag{2}$$

where R_n is the net radiation measured above the vegetation, L_e is the latent heat of evaporation $[J/kg]$, E is the evaporation rate $[kg/s/m^2]$ and H is the sensible heat flux at screen height. Notice that in the above equation we neglected the terms corresponding to the CO_2 flux, the energy advection into the layer and the energy storage within the leaves. An order of magnitude of the energy storage rate is computed in the Appendix of this paper and it is negligible.

One has to explicitly specify the net radiation input into the system R_n which represents the net radiation balance between short- and long-wave radiations at the earth surface (Brutsaert (2005)). For 30 of the analyzed 32 FLUXNET sites, the value of R_n was measured at a half-hour time step. Hence, no model was necessary for the computation of R_n. However, for sites no. 5 and 6 in Table 1 (deciduous temperate forests), the net radiation was not measured. Instead, the global short-wave radiation, R_s, was provided at a half-hour time step. We computed the net radiation R_n using the following simple model (Dingman (2002)):

$$R_n = R_s\left(1-\alpha_v\right) + \epsilon_v\left(\epsilon_{at}\sigma T_a^4\right) - \left(\epsilon_v \sigma T_v^4\right) \tag{3}$$

where T_v and T_a are the vegetation and air temperatures $[K]$, respectively, α_v is the albedo of the vegetation, ϵ_v is the emissivity of the vegetation and ϵ_{at} is the integrated effective emissivity of the atmosphere and canopy. We considered that $\alpha_v \approx 0.15$, value which closely corresponds to the albedo of a deciduous forest (Brutsaert (2005)). For the emissivity of the vegetation we considered that $\epsilon_v = 0.97$ (Brutsaert (2005)). The model of Kustas et al. (1994) was used in this study for ϵ_{at}. For cloudy conditions ϵ_{at} is determined from the degree of cloud cover, C. An average value of 0.5 was chosen for C.

E and H in equation 2 can be written with respect to the mean variables defining the vapor/heat transfer processes at the earth surface. The water vapor diffuses out of the stomatal cavities overcoming the stomatal resistance r_s, and is then transported by means of the turbulent air flow towards the

atmosphere. This turbulent transfer can be characterized with an aerodynamic resistance r_a. In this respect, the evaporation rate can be written as follows:

$$E = \rho_a \frac{1}{r_a + r_s} \left(q_v^* - q_a\right) \tag{4}$$

where ρ_a is the dry air density $[kg/m^3]$, r_a and r_s are the aerodynamic and stomatal resistances, respectively $[s/m]$, q_v^* is the specific humidity in the stomatal cavities $[kg_{vapor}/kg_{dryair}]$ and q_a is the mean air specific humidity at the level of measurement. The specific humidity of the air depends on the air temperature T_a and water vapor pressure deficit, VPD $[kPa]$ (which are both available from the FLUXNET database at a half-hour time interval):

$$q_a = 0.622 \frac{e_a}{P - e_a} \tag{5}$$

where:

$$e_a = e_a^* - VPD \tag{6}$$

$$e_a^* = 0.611 exp\left(17.3 \frac{T_a}{T_a + 237.3}\right) \tag{7}$$

in which T_a is the air temperature in ^oC, e_a is the air vapor pressure $[kPa]$ and e_a^* is the air vapor pressure at saturation $[kPa]$. Since the air in the stomatal cavities is considered at saturation, q_v^* will only be dependent on temperature T_v of the vegetation.

The heat is transferred between vegetation and atmosphere by means of the turbulent flow over the vegetation cover, the only resistance opposing to this transfer being the aerodynamic resistance r_a. Hence:

$$H = \rho_a c_{pa} \frac{1}{r_a} \left(T_v - T_a\right) \tag{8}$$

where c_{pa} is the specific heat of the air $[J/kg/K]$ and T_a is the air temperature at the height of measurement.

At all FLUXNET sites, measurements of mean wind speed u and friction velocity u_* are provided. Hence, the resistance to momentum transport can be directly computed as $r_{am} = u{u_*}^{-2}$. However, since transfers of water vapor and heat from a rough surface encounter greater aerodynamic resistance than does the transfer of momentum (Thom (1972)) one has $r_a > r_{am}$. Verma et al. (1986) proposed a model for the "excess resistance" such that:

$$r_a = \frac{u}{{u_*}^2} + \frac{f}{u_*} \tag{9}$$

where $f = (2/k)\,(D_T/D_v)^{2/3}$ is a factor depending on the thermal (D_T) and molecular (D_v) diffusivities of water vapor and the von Karman constant ($k = 0.4$). One easily obtains that $f \approx 4.9$. The formulation in 9 was used here instead of the well known logarithmic profile approach because the friction velocity is measured at all FLUXNET sites. Notice, however, that one can easily prove that equation 9 is equivalent to the logarithmic profile approach. In equations 4 and 8, the aerodynamic resistances are identical because we assumed that the mechanisms underlying the transfer of the two scalars (heat and water vapor) are the same.

In the context of equations 4-9 equation 2 has a single unknown, the vegetation temperature T_v. Furthermore, all parameters needed to solve equation 2 (R_n, T_a, VPD, u_*, u,) are provided by the FLUXNET database excepting the stomatal resistance r_s.

Notice that in this study, we do not intend to model the instantaneous dependence of the stomatal resistance on external factors like water and light availability. Rather, we look at the stomatal resistance as a fixed parameter characterizing the average state of the vegetation. Therefore, for each site of the FLUXNET database we are fixing r_s and we are solving the balance equation 2 for a given period of time. In this way, we are able to investigate its influence on the thermal state of leafs and on the surface fluxes, E and H. Notice that an exact analytical solution of T_v in equation 2 cannot be obtained. Hence, a numerical solution is found using the classical secant method.

3 The optimal bioclimate with respect to the external constraints

In order to make an analysis of the optimal state of the vegetation one has to identify first the constraints which influence the development of plants. Two main resources are needed by plants in order to survive: water (needed to absorb nutrients from soil and to capture CO_2) and light (needed for the photosynthesis process). Another important constraint is related to heat. The heat is a major stress factor for plants since the photosynthesis is highly dependent on leaves temperature. Notice that we are analyzing the optimal state of the plants under potential conditions. Hence, the water constraint is eliminated from our analysis and we are left with the heat and the light constraints.

3.1 Heat constraint

The heat constraint is directly linked to the leaf temperature because the leaf temperature strongly influences the plant photosynthesis efficiency. Numerous studies have shown that plant productivity is highly dependent on leaf temperature (Berry and Bjorkman (1980); Larcher (1983a); Kramer and Kozlowsku (1960); Gates (1960)). For potential conditions (unlimited water), a given light intensity and for C3 plants, the typical dependence of the net photosynthesis, P $[g_{CO_2}/m^2/hr]$, with respect to the leaf temperature, T_v, is shown in Figure 1a. The main reason behind the strength of the dependence of plant productivity on T_v lies in the strong temperature dependence of all biochemical reactions involved in the photosynthesis process (Taiz and Zeiger (2002)). It is interesting to observe that P does not increase monotonically with T_v but has a maximum, P_m, at an intermediate optimum temperature, T_m. It is widely accepted that this optimal temperature has a strong genetic dependency and there are evidences that plants have adapted their optimal temperature to the local climate in order to function efficiently. In this context, it is not surprising that T_m can vary from a few degrees above zero for alpine and arctic plants to as much as 50 ^oC for plants living in deserts (Taiz and Zeiger (2002)).

Eagleson (2002) (pag. 240) identifies T_m as a determinant selection factor in the plant adaptation process to the local climate. Looking from the perspective of the Darwinian expression of vegetation function, Eagleson (2002) (pag. 249) proposes as a first condition for bioclimatic optimality with non-limiting water that plants need to adapt their optimal temperature T_m to the mean leaf temperature over the growing season $\overline{T}_v$ such that:

$$T_m \approx \overline{T}_v \tag{10}$$

In turn, $\overline{T}_v$ is highly dependent on the local climate (average air temperature $\overline{T}_a$, wind speed $\overline{u}$, and radiation influx $\overline{R}_n$) and stomatal resistance r_s (see equations 2, 4 and 8). By estimating that, for well watered plants, the difference between the air and leaf temperature is small ($= O(10^{-1})$ and the vegetation system is closely isothermal, Eagleson (2002) (pag. 167) assumed that the long-term average "big leaf" temperature, $\overline{T}_v$, is approximately equal to the atmospheric average temperature, $\overline{T}_a$:

$$\overline{T}_a \approx \overline{T}_v \tag{11}$$

Numerous experimental evidences exist to support the above statement (Gates et al. (1968); Monteith (1973); Larcher (1983b)). More recently, using an ex-

tremum principle to the evaporation, Wang et al. (2007) theoretically shows that the average evaporation process from the soil-vegetation system should be close to an isothermal process.

The statements in equations 10 and 11 lead Eagleson (2002) to formulate the *heat proposition* for bioclimate optimality, namely:

$$T_m \approx \overline{T}_v \approx \overline{T}_a \tag{12}$$

A first validation of this proposition was done in Eagleson (2002) (Fig. 9.4, p. 281) by evidencing that, for several tree species coming from different climates, one has indeed $T_m \approx \overline{T}_a$.

In this study we will attempt to further analyze this hypothesis and to validate it using the FLUXNET meteorological database.

3.1.1 The stomatal regulation and the thermal state of leaves

The adaptation of T_m to the local climate ($\overline{T}_a$) is mainly made by a genetic mechanism and thus it implies a very large time scale. On the other hand, the condition $\overline{T}_v \approx \overline{T}_a$ could be fulfilled if only the leaf can actively regulate T_v. It is well known (Taiz and Zeiger (2002)) that, due to the high latent heat of vaporization of water, the main mechanism for leaf temperature regulation is the control of the transpiration rate. This in turn is mainly done by stomatal resistance modulation. The energy balance at the leaves surface, equation 2, states that the net energy input form the sun is partially used to evaporate the water, E, transported by the plant structure to the leaves, while the rest is evacuated into the atmosphere as residual sensible heat H.

Plant have interest in controlling E because the water vapor flux has a tremendous influence on all vital plant physiological processes. Firstly, the CO_2 uptake, needed for the photosynthesis process, is highly correlated with E (Larcher (1997); Eagleson (2002); Taiz and Zeiger (2002)). Indeed, the paths of the CO_2 and water vapor diffusion processes are the same: atmosphere - stomatal openings - intercellular air - water of the mesophyl cell walls, for CO_2, and reverse for the water vapor. Hence, the resistances opposing the two diffusion processes are roughly the same. Among them, the stomatal resistance is the largest one. This poses a functional dilemma (Taiz and Zeiger (2002)) to the leaf since a decrease in stomatal resistance through the opening of stomata favors CO_2 uptake but is unavoidably accompanied by substantial water loss. And even slight water deficits within the leaf cause severe malfunctioning of many cellular processes (Taiz and Zeiger (2002)). In this respect, the main objective of the leaf is to adapt the photosynthesis capacity to the photosynthetically active radiation PAR, while the main constraint on the leaf is to

judiciously balance the water losses and water gains.

Hence, any leaf needs to carefully correlate its water loss by transpiration, E, to the water flux extracted from the soil, W. The influx W is the flux of liquid water per unit leaf area in the xylem, $[kg/s/m^2]$. Notice that E is a measure of the atmospheric demand for evaporation, while W is a measure of the plant water transport capacity. On a day-to-day scale, plants always adapt the evaporation demand with their transport capacity such that:

$$\overline{E} \approx \overline{W} \tag{13}$$

where the average bar denotes the averaging procedure. The above equation is no more than the quasi-steady state of the evaporation flux (Hubbard et al. (1999)). To identify the mechanism behind the equilibration of the leaf water balance one has to identify first the factors influencing E an W.

On one hand, the atmospheric demand E, through the balance equation 2, is dependent on R_n, wind speed, u, vapor pressure deficit, VPD and the stomatal resistance, r_s. Obviously, among these factors, only r_s can be directly modified by plants. Thus, the mechanism for adapting E to W is the modulation of the stomatal resistance r_s.

On the other hand, the water flux W depends on the hydraulic conductance of the flow path form the soil to leaf (K_L $[kg/s/m^2/MPa]$) and the water potential difference between the leaf (Ψ_l $[MPa]$) and the soil (Ψ_s $[MPa]$), adjusted for the gravitational potential (Hubbard et al. (1999); Tuzet et al. (2003); Phillips et al. (2002)):

$$W = K_L \left(\Psi_s - \rho g h - \Psi_l\right) \tag{14}$$

where h is the plant height. The mechanisms behind the variation of W are complex. Firstly, the hydraulic conductance K_L is fixed by the plant structure. Indeed, under the assumption of negligible xylem cavitation, K_L depends on the following structural parameters: the flow length path, L, the sapwood permeability, k_s and the sapwood cross-sectional area per unit leaf area A (Pothier et al. (1989); Reid et al. (2005)). Although there are evidences that under draught conditions K_L decreases due to xylem cavitation (Sperry (2000)), it is still unclear if this decrease is deliberately controlled by plants or is just a consequence of plant exposition to a high water stress. Secondly, following the arguments of the cohesion-tension theory (Steudle (1995); Tyree (2003)), the low leaf water potential needed for the ascent of water towards the leaves is created at the air-water interfaces within the walls of the mesophyl cells. As water evaporates from the surface film that covers the cell wall of the mesophyll, water withdraws farther into the interstices of the porous cell wall and

the water surface tension increases the negative pressure in the liquid phase (Taiz and Zeiger (2002)). Hence, Ψ_l is directly correlated to the water content of the leaf θ $[kg]$ in a similar way as the soil water characteristic curve correlates the soil suction with the degree of soil saturation. This porous media behavior of the mesophyl spongy tissue is supported by several experimental studies (Lang et al. (1969); Cowan (1972)) which shows a direct correlation between the water content of the leaf, θ, and the leaf water potential Ψ_l

In turn, the water content of the leaf, θ is directly linked to E and W through the water balance of the leaf:

$$\frac{d\theta}{dt} = (W - E)\, S_l \tag{15}$$

where S_l is the leaf surface. The above equation shows that in order to actively control Ψ_l leafs have to act on the leaf water content θ. This can be only done by modulating E with respect to W.

When coupled to the constraint in equation 13, equation 15 highlights the strong link between E and W: a variation in the atmospheric demand E made by a stomatal resistance modulation will be reflected in a modification of the water transport capacity W by means of the leaf water content. As well, a modification of W (by a variation of the soil water potential for example) will be followed by an adaptation of E (by means of the stomatal resistance modulation) such that the quasi-steady state in equation 13 is maintained. Looking now at the main parameters influencing E (R_n, u, VPD, r_s) and W (K_L, Ψ_s, $\Psi_l = f(\theta)$, h) one can observe that the modulation of the stomatal resistance is the main mechanism by which leafs can adapt to the varying external constraints (R_n, u, D, Ψ_s). Notice as well that controlling the leaf water content also helps plants to minimize xylem cavitation by maintaining a minimum leaf water potential Ψ_l^{min}.

The balance equation 2 coupled with equations 4 and 8 shows that r_s has a significant effect on the evaporation rate and the sensible heat flux at the leaf surface. To quantitatively analyze this influence, it is instructive to approximate the solution of the balance equation 2 which does not have an analytical solution for the vegetation temperature T_v. However, the approximation of Penman states that:

$$\frac{e_v^* - e_a^*}{T_v - T_a} \approx \left(\frac{de^*}{dT}\right)_{T_a} = \Delta \tag{16}$$

where e_v^* and e_a^* are the vapor pressures at saturation $[kPa]$ corresponding to the vegetation temperature T_v and the air temperature T_a respectively and

$\Delta = (de^*/dT)_{T_a}$ is the slope of the saturation vapor pressure taken at the air temperature. Using the above approximation one can easily obtain that:

$$T_v - T_a \approx \frac{R_n - \frac{L_e \rho_a}{r_s + r_a}(q_a^* - q_a)}{\frac{\rho_a c_{pa}}{r_a} + \frac{L_e \rho_a}{r_s + r_a}\frac{0.622}{P}\Delta} \tag{17}$$

Now we can analyze the above equation for the two limits: $r_s \to \infty$ and $r_s \to 0$. When r_s is very large the evaporation process is penalized and $E \to 0$. Therefore, the net energy input at the leaves surface R_n will be transferred back to the atmosphere as sensible heat H. The leaves are overheated and the leaves temperature, T_v will be higher than the air temperature, T_a:

$$T_v - T_a \approx \frac{R_n}{\frac{\rho_a c_{pa}}{r_a}} \ (> 0) \tag{18}$$

When r_s is very small (approaching zero), the evaporation process is favored. If the turbulent transfer is strong enough (r_a is small) the water flux evaporated in the stomatal cavities will act as a heat sink which counteracts the natural tendency of the sun to heat the leaves. Looking at equation 17, one expects that, for this limiting case, the temperature of the leaf to decrease below the air temperature since for small r_a:

$$R_n - \frac{L_e \rho_a}{r_a}(q_a^* - q_a) < 0 \tag{19}$$

We conclude thus that by acting on r_s leaves dispose of an important mechanism for both modulating the water vapor flux E and regulating their temperature T_v. More importantly, if the turbulent transfer capacity of the atmosphere is intense, a critical stomatal resistance r_s^T exists such that the vegetation and the air temperatures becomes equal: $T_v = T_a$.

The model presented in section 2 will now be used to analyze the influence of the stomatal resistance on the evaporative and thermal state of plants. As already stated, we are fixing the stomatal resistance r_s and we solve the balance equation for the growing season. We will prove in the "Results" section that, for all analyzed FLUXNET sites, a critical stomatal resistance $\overline{r}_s^T$ exists such that *the average* air and vegetation temperature (averaged over the growing season) becomes equal: $\overline{T}_v = \overline{T}_a$. This is very important since this state corresponds precisely to the optimal plant state defined by Eagleson's heat proposition in equation 12.

One interesting observation can be made about the state defined by $\overline{r}_s^T$. Since H is proportional to $T_v - T_a$ (equation 8) it is easy to see that the state

defined by to $\overline{T}_v = \overline{T}_a$ will also minimize the average sensible heat flux $\overline{H}$ (averaged over the growing season). Hence, when $\overline{T}_v = \overline{T}_a$ one also obtains that $\left(\overline{H} << L_e\overline{E}\right)$. In this respect, the optimal thermal state of plants defined by $\overline{r}_s^T$ is characterized over a long period of time by:

$$\overline{R}_n \approx L_e\overline{E} \tag{20}$$

where the overbar denotes the averaging operator over the considered time scale. This will clearly be displayed by the numerical results obtained throughout section 4. Equation 20 is very important since it points out that, *given potential conditions, optimal plants will favor evaporative conditions such that the net energy input into the system to be almost entirely evacuated in the atmosphere as latent heat flux.*

3.2 Light constraint

It is well known that the net insolation level, I, has a significant influence on the plant net photosynthesis P (CO_2 assimilation rate). For a given ambient temperature and given potential conditions the *light response curve* of a given plant has a typical variation as shown in Figure 1b. In the dark ($I = 0$), the productivity is negative because CO_2 is given off by the plant due to respiration. With the initial increase of I the plant increases proportionally the productivity. The critical radiation level, I_{cp}, at which $P = 0$ is called light compensation point. This radiation level varies from one specie to another and reflects an adaptation of the plant to the average insolation level: plants grown in full sunlight have a larger I_{cp} compared with plants grown in the shade (Taiz and Zeiger (2002)). Increasing further I results in a proportional increase in productivity. However, there is a critical radiation level, I_{sl}, above which the plant productivity remains constant at the level of P_m. As one clearly expects P_m reaches a maximum for the optimal temperature T_m. This level is the light-saturated rate of photosynthesis. Finally, if I increases above the limit I_{sw} the plant productivity decreases to zero.

The plant state located on the linear increase in productivity is usually called a *light limited state* since more light will stimulate more photosynthesis. The flat productivity rate above the saturation level I_{sl} is commonly referred to as CO_2 *limited*, indicating that biochemical factors other than incident light becomes limiting to photosynthesis (Taiz and Zeiger (2002)).

There is a clear experimental evidence that the light saturation level I_{sl} is adapted by each plant to the environmental net insolation level, I_0, to which the leaf is exposed during the growth (Harvey (1979)). What is remarkable is

that this adaptation can be made at the time scale of the plant life. Indeed, it was shown (Björkman et al. (1981)) that the same specie grown at different insolation levels (for example in the shade or in full sunlight) adapted I_{sl} to the level of I_0.

Eagleson (2002) (p.249) analyzed the light constraints on plants from an ecological point of view, hence at a much larger time scale than the study of Björkman et al. (1981). The plant state defined by $I_{sl} < I_0$ was identified as non-optimal because the residual insolation $I_0 - I_{sl}$ remains unused by the plant and competition among species will favor species having a I_{sl} close to the environmental insolation level I_0. On the other hand, the state $I_{sl} > I_0$ puts a stress on plant development due to insufficient light and associated risk of trauma during transient periods of lower insolation. In this context, Eagleson (2002) hypothesis is that the optimal light state of plants, given potential conditions, will be defined by:

$$I_{sl} \approx I_0 \tag{21}$$

This is the *light proposition* for bioclimate optimality. This hypothesis was tested and validated in Eagleson (2002) (p. 283) for several tree species coming from different climates.

3.2.1 I_{sl} - a measure of the maximum water transport capacity of plant

In the following we use the conclusions derived in section 3.1 concerning the optimal thermal state of plants in order to demonstrate the link between the maximum water transport capacity of plant and the critical insolation level I_{sl}.

In Figure 1b the linear increase in productivity with the insolation level can be approximated with the biochemical assimilation capacity function:

$$P \approx \epsilon I \tag{22}$$

where the slope $\epsilon\,[g_{CO_2}/MJ]$ depends on the maximum quantum yield of photosynthesis (Taiz and Zeiger (2002); Eagleson (2002)) and reflects the efficiency of the leaf to use the photon influx for CO_2 assimilation. For C_3 plants an average value for ϵ is 0.81 g_{CO_2}/MJ (Eagleson (2002)). If we assume now that potential conditions are met and that plant is optimal with respect to the heat constraints imposed by the local environment, then the heat proposition in equation 12 will be valid. As pointed out in section 3.1.1 this also means that $\left(\overline{H} << L_e\overline{E}\right)$. Using now the energy balance at the leaf surface,

$I \approx \overline{H} + L_e\overline{E}$, equation 22 becomes:

$$P \approx \epsilon L_e \overline{E} \tag{23}$$

The equivalence between equations 22 and 23 is very important and has a two fold interpretation. On one hand it reveals that the net productivity of *optimal plants* is related to insolation energy influx and to the latent transpiration flux with the same degree of strengthness. This means that, by adapting $L_e\overline{E}$ to I, optimal plants are adapting their processing capacity of the CO_2 (which depends on the light influx) to the availability of CO_2 (which is directly linked to the transpiration flux).

Another important aspect is revealed by equations 22 and 23. As noted in section 3.1.1, $\overline{E} \approx \overline{W}$, hence equation 23 is also equivalent with: $P \approx \epsilon L_e \overline{W}$. We noticed that, to avoid xylem cavitation the leaf is constraint to maintain a minimum water leaf potential Ψ_l^{min}. Hence, each plant will be characterized by a maximum water transport capacity from the roots to the leaves, W_m. In this respect, when I increases, the transpiration rate, $\overline{E}$, will be able to follow up until the maximum limit $E_m \approx W_m$ is reached.

Hence, the productivity rate P is limited to its maximum value, P_m, by two mechanisms. On one hand P can be limited by factors which are directly linked to the biochemical process involved in photosynthesis like electron transport rate, rubisco activity or the metabolism of triose phosphates (Taiz and Zeiger (2002)). On the other hand photosynthesis can reach saturation if the maximum water transport capacity of the plant W_m is reached.

We believe that the water transport capacity is just as important in limiting the photosynthesis rate as the biochemical factors. To argue this statement we rely on the evidence (Harvey (1979); Björkman et al. (1981)) that the biochemical processes involved in photosynthesis can be rapidly adapted by plants at the time scale of plant life such that the saturation level I_{sl} will closely correspond to the average insolation level during the period of growth, I_0. On the other hand, W_m, can hardly be adapted at the time scale of plant life since, as already noticed, W_m depends on parameters fixed by the plant structure (K_L, Ψ_l^{min}, h) which can be mainly adapted by plants through a genetic mechanism.

In this context we will assume that a given plant has adapted the biochemical processes of the photosynthesis to the local average level of insolation I_0. This means that, given sufficient water transport capacity, the leaf can sustain a maximum net productivity $P_m = \epsilon I_{sl} \approx \epsilon I_0$. Now, if the plant has a small W_m such that $L_e E_m \approx L_e W_m < I_0$, the plant productivity will be limited by W_m to the level $P_w = \epsilon L_e E_m$ which is smaller than the leaf photosynthetic

capacity P_m. This means that the plant water transport structure is under-dimensioned with respect to the environmental constraint I_0. In this context, the plant has a net disadvantage compared with plants that have adapted P_w to P_m. On the other hand if the plant has a large water transport capacity such that $L_e E_m \approx L_e W_m > I_0$ then $P_w > P_m$ and the productivity will be limited by the biochemical processes at the level of P_m. The plant has a water transport capacity which is over-dimensioned with respect to the climate constraint embodied here by $P_m \approx \epsilon I_0$. The plant is put under environmental stress because it wastes resources to develop a water transport architecture that will never be used at full capacity. Again, competition among species will favor plants that have a water transport capacity adapted to P_m. In this respect it is clear that competition among species will force plants to adapt W_m to I_0 such that:

$$P_m = \epsilon I_{sl} \approx \epsilon I_0 \approx \epsilon L_e W_m \tag{24}$$

From this point of view large insolation rates I_0 such that $I_0 >= I_{sl}$ are both water transport limited and CO_2 limited conditions despite the potential conditions at the plant roots. That is because the transpiration demand cannot be sustained by both plant water transport configuration and leaf photosynthesis capacity.

Now, if $I_0 > I_{sl}$ the plant will only be able to use a fraction of the available energy, i.e. I_{sl} because it cannot increase the evaporation rate beyond $\overline{E}_m \approx W_m$. Hence, the excess of energy at the leaves surface $(I_0 - I_{sl})$ will be evacuated in the atmosphere as sensible heat flux, increasing the leaves temperature. One expects that if I_0 increases much above the value of I_{sl} the overheating of the leaves will shift the state of plants from the optimal state characterized by $T_m \cong \overline{T}_v$, determining a decrease in the productivity. Hence, above a critical insolation level, I_{sw} (see Figure 1b), one expects that the productivity will start to decrease below its maximum P_m. It is interesting to notice that Eagleson (2002) identified I_{sw} as the radiation limit above which soil desiccation becomes important, the roots access to water becomes restricted and the leaves start to react to these dry conditions. Although this is true, we believe that, given potential conditions, I_{sw} must also be seen as the insolation limit above which the productivity decreases due to an overheating of the leaves.

4 Results and discussion

Our aim here is to validate the hypothesis stated in section 3.1 that given potential conditions, plants adapt their stomatal resistance such that over the growing season the average leaf and air temperature are equal. We will

try to compare the numerical results obtained with the model described in section 2 with the experimental data provided by the FLUXNET network. As already pointed out, the only unknown parameter of this model is the surface resistance to evaporation r_s. Although r_s has high daily and seasonal variability, in this model we are only interested in the average state of the vegetation. In this light, r_s is fixed and has the meaning of an average surface resistance of the canopy over a longer period of time. With r_s fixed, and using the meteorological data provided by the FLUXNET network, we solve the energy balance equation at the leaf surface (equation 2) to obtain the vegetation temperature T_v and the surface fluxes E and H. In this way we are able to investigate the influence of the canopy surface resistance r_s on T_v, E and H. Finally, we will identify among the whole series of measurements, those conditions which closely correspond to potential conditions and we will show that the state corresponding to $\overline{T}_v \approx \overline{T}_a$ closely corresponds to the potential state of plants.

The FLUXNET network provides a comprehensive set of meteorological and surface fluxes data from sites of various climates and biomes (Baldocchi et al. (2001)). On one hand, meteorological measurements of above-canopy temperature, humidity, wind speed and net radiation are provided. On the other hand, vapor (E) and heat (H) fluxes as well as the vertical CO_2 flux, are computed from the mean covariance between fluctuations of vertical velocity (w') and the respective scalar: water vapor, temperature and CO_2 concentration. We analyze in this study all 32 sites within the FLUXNET Marconi conference gap-filled flux and meteorology database. The sites are summarized in Table 1. Since the interaction between the biosphere and the atmosphere varies significantly with the vegetation type, we divided these sites into five different biomes: deciduous forest, evergreen forest, evergreen Mediterranean climate, agricultural crops, grasslands and tundra.

Since the conclusions drawn from the application of the hypothesis of optimal bioclimate in section 3 are valid for an active vegetation cover we will restrict the period of research to the spring-autumn period, between Julian day 121 and 273. The only exception is made for site no. 7 which is located in the Southern hemisphere and in a tropical zone, thus the whole year is taken into account in this case. Moreover, the study period is also limited to daytime fluxes, which was defined as the period when the net radiation is positive ($R_n > 0$). This restriction was justified by the fact that during the night the processes controlling surface exchanges are different compared with daytime (Mahrt (1999)) and because heat fluxes are much larger during the day than during the night. Furthermore, there is strong evidence that the eddy covariance measuring method is less reliable during nocturnal periods (Lavigne et al. (1997); Law et al. (2001)).

4.1 The energy balance closure at FLUXNET sites

It is noteworthy that a meaningful comparison between numerical and measured surface fluxes can only be made if the experimental surface fluxes verify the energy balance equation 2. In this context, an investigation of the energy balance closure at FLUXNET sites was assessed first.

In Figure 2a, we plot R_n versus $H^* + L_e E^*$ for site no. 15 in Table 1. One can easily detect an imbalance between the net radiation input and the latent and sensible heat fluxes. This has already been evidenced in Wilson et al. (2002) where a mean 20% imbalance was detected for all 22 FLUXNET sites that they studied. The main conclusion in Wilson et al. (2002) was that, most probably, the turbulent fluxes of sensible heat and latent heat were underestimated. We investigated the energy imbalance for all sites presented in Table 1 and we observed the same pattern: on average R_n is always larger than $H^* + L_e E^*$. We quantified this imbalance by computing a correction coefficient, $f_c > 1$, such that the energy balance equation, averaged over the whole measuring period, is verified:

$$\overline{R_n/f_c - H^* - L_e E^*} = 0 \tag{25}$$

Notice that hereafter only site no. 15 will be presented in detail since the results for all other sites are very similar. For all other sites only the main numerical results are summarized in Table 2. For site no. 15, we obtained $f_c = 1.48$. In Figure 2b, the corrected net radiation is plotted against the latent and sensible heat fluxes for site number 15. As one can see, the correlation between R_n/f_c and $H^*+L_e E^*$ is significant ($R^2 = 0.8$) suggesting the existence of a systematic relative error in the measuring of the turbulent surface fluxes. The correction factor f_c and the corresponding correlation coefficient R^2 were computed for all sites in Table 1 and the results are summarized in Table 2. For deciduous and evergreen temperate forests, the mean imbalance is of order of $30\% - 40\%$ ($\overline{f}_c = 1.4$). This imbalance is lower ($10\% - 20\%$) for agricultural crops, grasslands and tundra sites. It is important to notice that the correlation coefficient between R_n/f_c and the sum $L_e E^* + H^*$ is very good for almost all sites suggesting that there is a constant relative error in the underestimation of the surface fluxes. In Figure 3, we plotted f_c against the correlation coefficient R^2_{fc}. One easily observe that to an increase in f_c corresponds to a decrease in the correlation coefficient R^2_{fc}. This result suggests that measurements made for sites with large energy unbalance should be regarded with less confidence. Basically, we can identify six sites characterized with large unbalance and/or poor correlation coefficients: sites no. 5, 8, 9, 12, 17, 24 and 32.

In this context, in order to have a meaningful comparison between the mea-

sured and the numerical surface fluxes, the energy balance equation to be solved has to be coherent with the corrected energy balance equation 25. Hence, instead of equation 2 we will solve numerically the following corrected equation:

$$R_n/f_c - H - L_eE = 0 \tag{26}$$

where R_n is the measured net radiation at the canopy level and L_eE and H are respectively the latent and sensible heat flux expressed in equations 4 and 8.

4.2 The actual state of the canopy ($\overline{r}_s$)

By fixing r_s in our model and keeping it constant along the growing season we can analyze the influence of r_s on H and E. In this context it would be interesting to find the critical surface resistance $\overline{r}_s$ such that the obtained numerical surface fluxes best fit the measured data. This can be done by computing the average error (averaged over the growing season) between the measured (E^* and H^*) and computed (E and H) surface fluxes and this for each distinct r_s:

$$\begin{aligned} \epsilon_{LE} &= \frac{1}{N}\sum_{i=1}^{N}(L_eE_i - L_eE_i^*) \\ \epsilon_H &= \frac{1}{N}\sum_{i=1}^{N}(H_i - H_i^*) \end{aligned} \tag{27}$$

where N is the number of measurements over the analyzed period of time. In Figure 4a, the errors ϵ_{LE} and ϵ_H are plotted against the surface resistance r_s for site no. 15. One can easily observe that there are two characteristic surface resistances r_s^E and r_s^H which cancel out the mean errors ϵ_{LE} and ϵ_H, respectively. Hence, r_s^E and r_s^H describe the mean evaporative and thermal state of the vegetation over a long period of time. In Figures 5a and 5b, we plotted the modeled surface fluxes, corresponding to r_s^E and r_s^H respectively, against the measured surface fluxes, E^* and H^*. As shown the correlations between the numerical and actual surface fluxes are significant ($R_E^2 = 0.48$, $R_H^2 = 0.58$, see Table 2). Moreover, the fact that $r_s^E \approx r_s^H$ comes to support the hypothesis that the vegetation can be described, on average and over a long period of time, with a unique average surface resistance $\overline{r}_s$:

$$\overline{r}_s \approx r_s^E \approx r_s^H \tag{28}$$

Looking at Figure 4a, we observe that, for $r_s > \overline{r}_s$, the computed evaporation becomes smaller than the measured one ($\epsilon_{LE} < 0$) because a larger surface resistance is opposing to the vapor transfer at the leaf surface. Consequently, the heat sink at the surface of the leaves is weakening, favoring heating of the vegetation and thus increasing the sensible heat flux ($\epsilon_H > 0$). If $r_s < \overline{r}_s$ the reverse is happening: the evaporation is intensified with respect to the measured one and a large latent heat extraction will counteract the heating of the leaves, decreasing thus the sensible heat flux with respect to the measured case.

We computed r_s^E, r_s^H, R_E^2 and R_H^2 for all sites, see Table 2. One can observe that overall $r_s^H \approx r_s^E$ (see Figure 6) and that the correlation coefficients between modeled and measured surface fluxes, R_H^2 and R_E^2, are significant. This is very important since it proves that, although the stomatal resistance undergoes important variations at the daily and seasonal scales, one can satisfactorily describe the canopy over a long period of time with a unique average surface resistance $\overline{r}_s \approx r_s^H \approx r_s^E$. However, there are some exceptions to this result, sites no. 5, 8, 12, 24 and 32 for which $r_s^H \neq r_s^E$ and/or the correlation coefficients R_H^2 and R_E^2 are weak. This result was expected since, as already pointed out in the previous subsection, the same sites were characterized with a large energy imbalance and/or weak R_{fc}^2 coefficients.

One can notice the difference in $\overline{r}_s$ between different biomes. The smallest $\overline{r}_s$ was obtained for deciduous forests ($\approx 130\ s/m$). The $\overline{r}_s$ for evergreen temperate forest is larger suggesting that this type of vegetation cover is evaporating less than deciduous forest. The $\overline{r}_s$ for Mediterranean forest is even larger. This was expected since the dry conditions characterizing this climate will most probably determine an average state of vegetation considerably different from potential conditions. The $\overline{r}_s$ for agricultural crops and grasslands are close, whereas the $\overline{r}_s$ characterizing the tundra environment is smaller and of the same order of magnitude of the deciduous forest. It is noteworthy that, the obtained values of $\overline{r}_s$ in Table 2 are of significant importance since they can be now used to estimate the AET directly using the "one-step approach" introduced by Shuttleworth (2006).

4.3 The quasi-isothermal state of the canopy ($\overline{r}_s^T$)

One main concept arises from section 3.1.1: the average optimal thermal state of plants given potential conditions can be quantified by means of the critical stomatal resistance $\overline{r}_s^T$ such that the canopy and the air temperatures are on

average equal over the growing season. To show this state, we computed the average difference between the temperatures of the vegetation and the air:

$$\begin{aligned}\epsilon_T &= \overline{T_v - T_a} \\ &= \frac{1}{N}\sum_{i=1}^{N} T_{vi} - T_{ai}\end{aligned} \tag{29}$$

where the average operation is made over the entire study period. The variation of ϵ_T with respect to the surface resistance r_s is plotted in Figure 7 for site no. 15. One can see that there is a critical surface resistance, $\overline{r}_s^T$ for which $\epsilon_T = 0$, that is a surface resistance corresponding to a state where the vegetation temperature and the air temperature are equal *on average* over the growing season. The critical surface resistance $\overline{r}_s^T$ was computed for all sites and a summary is presented in Table 2. Notice that, the existence of $\overline{r}_s^T$ was already anticipated in section 3.1.1. For $r_s < \overline{r}_s^T$ the evaporation process is intensified, the vegetation is cooled with respect to the air temperature ($\epsilon_T < 0$) and the sensible heat flux, $\overline{H}$, is negative. On the other hand for $r_s > \overline{r}_s^T$ the evaporation is penalized and, the vegetation cover will overheat with respect to the air temperature ($\epsilon_T > 0$), determining a positive and increasing $\overline{H}$. As one can easily observe, excepting the tundra environment, $\overline{r}_s^T$ varies between 40 and 120 s/m. For tundra sites there is no critical stomatal resistance, $\overline{r}_s^T$, such that $\epsilon_T = 0$. In fact, for a zero stomatal resistance, the tundra vegetation still has an average temperature larger than the air temperature ($\epsilon_T > 0$). The reason behind this could reside in the different meteorological parameters of the artic environment. In fact, as equation 17 reveals, $\overline{r}_s^T$ is sensitive to the average net energy input at the leaf surface ($\overline{R}_n$) and to meteorological parameters like the average relative humidity and the average air temperature. $\overline{r}_s^T$ decreases when the average relative humidity increases. This may explain in part the results for the tundra biome since we observed that this environment is characterized with high relative humidity ($\overline{\phi} \approx 70\%$).

To quantify the influence of the surface resistance r_s on the average sensible and latent heat fluxes we computed for each r_s, $\overline{H}$ and $L_e\overline{E}$, averaged over the whole analyzed period of time. In Figure 8, the influence of r_s on $\overline{H}$ and $\overline{E}$ is showed for site no. 15. The constant averaged net radiation $\overline{R}_n/f_c$ and the variation of ϵ_T are also displayed in Figure 8. Notice that, from the energy balance equation 26, one has $\overline{R}_n/f_c = \overline{H} + L_e\overline{E}$. As one expected from the definition of H, $\overline{H}$ and ϵ_T become zero for the same critical stomatal resistance $\overline{r}_s^T$. One can easily observe that $\overline{r}_s^T$ divides the average plant state into two distinct regimes. On one hand, for $r_s > \overline{r}_s^T$ the plant is evaporating less than the net solar energy input ($L_e\overline{E} < \overline{R}_n/f_c$) and the energy excess is evacuated into the atmosphere as sensible heat flux, ($\overline{H} > 0$). This regime

would characterize a plant under non potential conditions, hence under a state of limited access to water. On the other hand, for $r_s < \overline{r}_s^T$ the plant is favoring an intense transpiration ($L_e\overline{E} > \overline{R}_n/f_c$) and consequently the leafs are cooled efficiently ($\overline{H} < 0$). In fact the plant evaporates more than the constraint imposed by the net solar energy input $\overline{R}_n/f_c$. As noted in section 3.2.1, this can be done only if the plant has a water transport capacity which is larger than the limit I_0/L_e imposed by the local insolation level. We noticed in section 3.2.1 that this situation is non-optimal because the plant is wasting resources for developing a water transport capacity which will never be used at full capacity. One expects therefore that the regime defined by $r_s < \overline{r}_s^T$ to be rarely encountered for optimal bioclimates. These interpretations come to support the hypothesis that, given potential conditions, the optimal thermal state of vegetation should closely correspond to the state defined by $\overline{r}_s^T$.

4.4 The potential state of the canopy ($\overline{r}_{sp}$)

To validate the hypothesis that the potential state of vegetation corresponds to the optimal thermal state defined by the surface resistance $\overline{r}_s^T$, we will analyze in the following only the periods of time that are likely to be characterized by potential conditions. The soil saturation is highly correlated with the precipitation events. It is well known (Eagleson (2002)) that for temperate climates the storm duration, m_{tr} is an order of magnitude smaller than the average inter-storm period, m_{tb}. During the inter-storm period the subsurface flow and the evapotranspiration are depleting the soil water. Hence, one expects that saturated soil conditions (potential conditions) to be mainly achieved during the storm period and shortly thereafter. In this respect, analyzed over a long period of time, plants are not functioning at potential conditions. This is nicely evidenced by the fact that $\overline{r}_s^T < \overline{r}_s$ (see Table 2). Assuming that $\overline{r}_s^T$ defines closely the potential state of vegetation, this result is coherent with the fact that, over a long period of time, the soil will exhibit a deficit of water and plants are not functioning at potential conditions.

In this context, it would be interesting to investigate the behavior of the vegetation cover shortly after the storm period, conditions which are supposed to be close to potential conditions (i.e., quasi potential conditions). One question remains to be answered: what is the time scale defining these humid conditions? The answer comes from the estimation of the average storm duration, m_{tr}. For a temperate climate the time scale of a typical storm is of order of 0.2 days (Eagleson (2002)). However, we are interested here in obtaining not only an estimate of high intensity storms which have small characteristic time scales but an order of magnitude of the average precipitation event characterizing each site. Hence, we should look for precipitations events having a larger time scale. We have chosen in this study a characteristic time scale of $m_{tr} = 24\ hrs$.

We believe this time scale is a good order of magnitude for the average rainfall. We computed the average rainfall by firstly making a moving sum of the precipitation series with a time window of order of m_{tr}. We obtained thus a time sequence of the precipitation cumulated over 24 hrs, PP $[mm/24h]$. Then we selected among this sequence the events which are characterized by a non-zero rainfall and we averaged them to finally obtain the average precipitation event, $\overline{PP}$ $[mm/24\ hrs]$. To select the measurements which are likely to correspond to potential conditions we have considered only the measurements following an average rainfall PP which is larger than $\overline{PP}$. Then, using the numerical model, we modeled the surface fluxes over the selected period by fixing the surface resistance r_s. Similar to the procedure described at section 4.2 we computed for the selected humid period an average error between the measured and the modeled surface fluxes:

$$\epsilon^p_{LE} = \frac{1}{N_s}\sum_{i=1}^{N_s}(L_eE_i - L_eE^*_i) \tag{30}$$

$$\epsilon^p_{H} = \frac{1}{N_s}\sum_{i=1}^{N_s}(H_i - H^*_i) \tag{31}$$

where N_s is the total number of the selected measurements. As one can see for site no. 15, the variation of ϵ^p_{LE} and ϵ^p_H (Figure 4b) is somewhat similar to the variation of ϵ_{LE} and ϵ_H in Figure 4a. However, the critical surface resistances r^E_{sp} and r^H_{sp} which cancel out the mean errors computed in equations 30 and 31 are significantly different from r^E_s and r^H_s which are computed for the whole series of measurements.

We computed r^E_{sp} and r^H_{sp} for all sites (see Table 2). As one can see there are 6 sites (no. 1, 7, 11, 12, 19, 25) for which this set of two parameters was not computed. This is because the precipitation data was missing or was too sparse. In addition, there is site no. 18 which lacked wind speed measurements rendering impossible the resolution of the present numerical model.

Since one expects that the energy balance equation 25 to be valid for the selected humid period as well, then r^E_{sp} should be approximately equal to r^H_{sp}. As presented in Figure 4b for the site no. 15 one has $r^E_{sp} \approx r^H_{sp}$. The difference between the two resistances is probably due to the fact that the energy balance closure during and shortly after an average rainfall is weaker compared with dry days. This hypothesis is also supported by the weak asymmetry between the variation of the two errors ϵ^p_{LE} and ϵ^p_H in Figure 4b. A possible reason for this imbalance may come from the fact that in writing 25 we have neglected the net energy input associated with inflows and outflows of water. This water-advected energy term may be quite important during and after a rainfall

(Dingman (2002)).

However, for the majority of sites analyzed in Table 2 we have obtained that $r_{sp}^E \approx r_{sp}^H$ suggesting that humid (potential) conditions can be characterized with a mean surface resistance:

$$\overline{r}_{sp} \approx r_{sp}^E \approx r_{sp}^H \tag{32}$$

There are exceptions to this rule: sites no. 4, 8, 9, 10, 16, 17, 22, 24 and 32. For sites no. 8, 9, 17, 24 and 32 this was an expected outcome since the same sites did not satisfy the energy balance equation over the entire measurement period. However, despite that for sites no. 4, 10, 16, 22 the energy balance closure over the entire study period was strong, r_{sp}^E was quite different from r_{sp}^H. As already mentioned, the probable reason behind this result is the neglection of net energy input associated with inflows and outflows of water. Notice as well that r_{sp}^E and r_{sp}^H are consistently smaller than r_s^E and r_s^H. This is expected since r_{sp}^E and r_{sp}^H should closely correspond to the potential state of the vegetation whereas r_s^E and r_s^H characterize the average actual state of the vegetation.

Let us compare now $\overline{r}_s^T$ with r_{sp}^E and r_{sp}^H. We eliminate from this comparison sites having a bad energy closure (over the entire study period as well as over the selected humid period) since we believe the level of confidence we can assign to the surface fluxes measurements for these sites is very low. Hence, sites no. 4, 8, 9, 10, 16, 17, 22, 24 and 32 were not taken into account. In Figure 9 we plotted $\overline{r}_s^T$ against $\overline{r}_{sp} = \left(r_{sp}^E + r_{sp}^H\right)/2$ for the remaining sites (no. 2, 3, 5, 6, 13, 14, 15, 20, 21, 23, 26, 27, 28, 29, 30 and 31). Notice that $\overline{r}_{sp}$ has a meaning only if $r_{sp}^E \approx r_{sp}^H$ which was indeed the case for the selected set of sites. As one can observe the optimal thermal state defined by $\overline{r}_s^T$ closely match the potential state defined by r_{sp}. Basically $\overline{r}_s^T$ is on average 15% smaller than $\overline{r}_{sp}$. This validates our hypothesis that, given potential conditions, plants are closely approaching the optimal thermal state defined by $\overline{r}_s^T$.

There are four exceptions from this rule in Figure 9, sites no. 20, 21, 30 and 31. We believe however that there is a strong reason for the atypical behavior of these four sites. Firstly, site no. 20 comes from Nordic latitude and a cold environment. More precisely this site is located within a boreal forest environment and a peatland. The vegetation of peatlands is a mixture of evergreen forest, i.e. vascular plants, and non-vascular plants, mainly moss (Admiral and Lafleur (2007)). The non-vascular plants have no tissues specialized for water transport like xylem or pholem. Consequently they have no real roots, stem or leaves. Our theoretical approach which takes into account the plant ability to modulate the water flux through the plant structure can only be applied to vascular plants. In this context the results for site no. 20 have to be regarded

with care. Moreover, it was shown that the hydrology of peatlands is very different from that of a typical forest (Admiral and Lafleur (2007); Lafleur and Roulet (1992)) and special care has to be taken when modeling the highly variable morphology of peatlands. Notice as well that the average state of plants for this site was defined by a large surface resistance ($\overline{r}_s \approx 300\ s/m$) and for a similar environment Admiral and Lafleur (2007) obtained the same order of magnitude for $\overline{r}_s$. Secondly there are sites no. 30 and 31 from an arctic environment, the tundra. The vegetation at these high latitudes is mainly characterized with non-vascular plants. In this context, we believe that these two extreme environments (peatlands and tundra) cannot be analyzed with the tools described in section 3.1. Finally site no. 21, comes from a needle-leaf forest. The reasons behind its atypical behavior remain for now unclear. However, the relatively high latitude characterizing this site and the climatic constraints associated with may explain in part this result.

In conclusion, the optimal thermal state and the potential state of the canopy are very close. In turn, the potential state of plants is very different compared with the actual state of canopy. This is well reflected by the following result:

$$\overline{r}_{sp} \approx \overline{r}_s^T < \overline{r}_s \tag{33}$$

4.5 The crop coefficient

In the light of the above findings, it would be interesting to analyze the shift between the potential state defined by $\overline{r}_s^T$ and the actual state of plants defined by $\overline{r}_s$. Excepting the tundra environnement which cannot be characterized with a valid $\overline{r}_s^T$, we computed for each site the ratio $r_{PET} = \overline{r}_s^T/\overline{r}_s$ where $\overline{r}_s$ was computed as the average between r_s^H and r_s^E. Then we computed the average of this ratio for each biome $\overline{r}_{PET}$ and the corresponding standard deviation, σ_{PET}. The results are plotted in Figure 10a. Note that in Figure 10a, sites no. 5, 8 and 12 were not included because $\overline{r}_s$ does not have a physical meaning due to the very large difference between r_s^E and r_s^H. We observe that $\sigma_{PET}/\overline{r}_{PET} < 30\%$ meaning that r_{PET} is homogeneous among each biome. This result is very important since it supports the physical soundness of the choice of $\overline{r}_s^T$ as the surface resistance characterizing potential conditions. Moreover $\overline{r}_{PET}$ is different among biomes suggesting that each type of vegetation interacts differently with the atmosphere. Deciduous forests have the largest $\overline{r}_{PET}$, meaning that the actual state of this biome is the closest to potential conditions. The average state of the evergreen forest is more distanced from the potential state than the deciduous forest. Even smaller $\overline{r}_{PET}$ are obtained for Mediterranean climate, an expected outcome due to the increase dryness of this climate. Agricultural crops and grasslands seem to have a similar be-

havior.

Finally, it is noteworthy that, asides from the tundra biome, $\overline{r}_s^T$ remains fairly constant among all sites at a level of $60-70\ s/m$. This result is not surprising since $\overline{r}_s^T$ is not directly dependent on the vegetation type but, as already pointed out, on meteorological parameters like $\overline{R}_n$, average relative humidity and air temperature which among all sites (except for the tundra sites) do not vary significantly.

Since $\overline{r}_s^T$ closely defines the potential state, we computed the crop coefficient k_p (see equation 1) corresponding to this state. Let us denote the potential surface fluxes, obtained for a surface resistance $\overline{r}_s^T$, by H_p and E_p. In this respect k_p will be the coefficient which cancels out the mean error of the difference between k_pE_p and the measured evaporation flux, E^*, that is:

$$\overline{k_pE_p - E^*} = 0 \tag{34}$$

We have computed the correlation coefficient R^2_{PET} between k_pE_p and E^* temporal series. Both k_p and R^2_{PET} are shown in Table 2. As one can easily observe for all sites the basic requirements for a physically sound k_p are met, that is:

$$\begin{aligned} &k_p < 1 \\ &k_p = O(1) \end{aligned} \tag{35}$$

Moreover, the obtained correlation coefficients R^2_{PET} (≈ 0.5) are significant, supporting the pertinence of the choice of the potential state as the state defined by $\overline{r}_s^T$.

We also computed an average crop coefficient, $\overline{k}_p$ for each biome and its corresponding standard deviation. These results are plotted in Figure 10b. As one can easily observe the crop coefficient is homogeneous among sites. This is important since one expected the crop coefficient to be relatively constant for a given biome. The variation of $\overline{k}_p$ with respect to biome type closely matches the variation of $\overline{r}_{PET}$ in Figure 10a.

4.6 Is the actual state of plants an optimal state too?

The above results point to the following statement: given potential conditions, highly evolved plants will reach an optimal bioclimate state defined by the heat proposition in equation 12.

We can place these results in a more general framework. Plants arrive at an optimal thermal state during the short potential conditions. However, due to the relative large interstorm period, water becomes an important stress factor for plants over a long period of time. Hence, during interstorms periods, plants will not be able to reach the optimal state and the plant average state will be shifted from the optimal potential state ($\overline{r}_s > \overline{r}_s^{min}$). We believe that the actual state defined by $\overline{r}_s$ should also be viewed as an optimal state of plants, given the water constraint. This is coherent with the results obtained by Wang et al. (2004, 2007) which stated that "land-atmosphere interactive processes lead to thermal and hydrologic states of the land surface that maximize evaporation in a given environment". Indeed, one expects that, given the water constraint, plants will choose an average surface resistance $\overline{r}_s$ which is as closest as possible to the optimal $\overline{r}_s^T$. From this point of view, plants appear to minimize $\overline{r}_s$ and thus, to maximize "locally" the evaporation rate. In this light the conclusion in Wang et al. (2004, 2007) would be a consequence of the fact that, given the water constraints, plants are straining to approach as much as possible the optimal state defined by the heat and light propositions (equations 12 and 21).

5 Conclusions

Following the approach developed by Eagleson (2002), we analyzed the optimal state of vegetation given the influence of the three major plant stresses: heat, light and water availability. The analysis of plants under heat and light constraints showed that, given potential conditions, the optimal vegetation state can be defined by the heat and light propositions (equations 12 and 21). We evidenced the importance of stomatal modulation for the thermal and water balance regulation of the leaf. We also identified that there is a critical surface resistance $\overline{r}_s^T$ which precisely corresponds to the optimal thermal state of plants, as defined by the heat proposition. By analyzing then the plant light response we showed that, in order to function optimally, plants need to adapt their water transport capacity to the local insolation constraint I_0.

To test the hypothesis relative to the heat proposition, we modeled the energy balance at the surface of the leaves. The input data for this model was provided by the FLUXNET network (Baldocchi et al. (2001)). The comparison between the numerical and the measured surface fluxes evidenced a characteristic stomatal resistance, $\overline{r}_s$, which corresponds to the average actual state of the canopy. Coupled with the "one step approach" introduced by Shuttleworth (2006), these characteristic stomatal resistances can be used to compute the actual evapotranspiration for different types of biomes.

We showed that plants can significantly thermoregulate their temperature

by means of the stomatal resistance and that there is a critical stomatal resistance, $\overline{r}_s^T$, corresponding to an average thermal state of plant such that $\overline{T}_v \approx \overline{T}_a$. We also showed that, for sites characterized with vascular plants, the optimal thermal state defined by $\overline{r}_s^T$ is indeed approached by plants when potential conditions are met. Since, $\overline{r}_s^T$ depends mainly on meteorological variables like R_n, T_a, vapor pressure difference and the aerodynamical resistance r_a, it would be interesting to evaluate in the future the influence of all these parameters on $\overline{r}_s^T$.

We evidenced that plants adopt a mechanistic behavior in response to external constraints: they adapt to achieve as much as possible an optimal state with respect to these constraints (heat, light, water). This is of great interest since research areas in both hydrology and ecology could use this optimum principle in their study of the complex soil-plant-atmosphere interactions.

6 Acknowledgments

This research was jointly funded by a grant from the Natural Sciences and Engineering Research Council (NSERC) of Canada (Collaborative Research and Development Program) and by OURANOS (Quebec Consortium on Regional Climate and Adaptation to Climate Change, www.ouranos.ca).

7 Appendix

One can estimate the order of magnitude of the energy storage rate, Q_{acc}, from the daily amplitude of the vegetation temperature, ΔT_v. Indeed, Q_{acc} can be expressed as:

$$Q_{acc} \cong \rho_v \; c_{pv} LAI h_l \frac{\Delta T_v}{\Delta \tau} \tag{36}$$

where ρ_v $[kg/m^3]$, c_{pv} $[J/kg/K]$ and ΔT_v $[K]$ are leaf density, leaf specific heat and daily amplitude of the vegetation temperature, LAI is the leaf area index (dimensionless), h_l is the average leaf thickness $[m]$ and finally $\Delta\tau$ is the time scale $[s]$ corresponding to the ΔT_v amplitude ($\cong 12\ hrs$). For typical values of leaf density (Witkowski and Lamont (1991)) ($\rho \approx 500\ kg/m^3$), leaf specific heat ($c_p \approx 3750 J/kg/K$), leaf area index (Eagleson (2002)) ($LAI \approx 5$) and leaf thickness ($h \approx 10^{-3}\ m$), one easily obtains that $Q_{acc} \approx 2\ W/m^2$, a negligible value with respect to the net energy input into the system, $R_n = O\left(10^2\ W/m^2\right)$.

References

Admiral, S., Lafleur, P., 2007. Modelling of latent heat partitioning at a bog peatland. Agricultural and Forest Meteorology 144, 213–229.

Allen, R., Smith, M., Perrier, A., Pereira, L., 1994a. An update for the calculation of reference evapotranspiration. ICID Bull, New Delhi 43, 1–34.

Allen, R., Smith, M., Perrier, A., Pereira, L., 1994b. An update for the calculation of reference evapotranspiration. ICID Bull, New Delhi 43, 35–92.

Baldocchi et al., D., 2001. FLUXNET: a new tool to study the temporal and spatial variability of ecosystem-scale carbon dioxide, water vapour and energy flux densities. Bull. Am. Meteorol. Soc. 82, 2415–2434.

Berry, J., Bjorkman, O., 1980. Photosynthetic Response and Adaptation to Temperature in Higher Plants. Annual Reviews in Plant Physiology 31 (1), 491–543.

Björkman, O., et al., 1981. Responses to different quantum flux densities. Encyclopedia of Plant Physiology 12A, 57–107.

Brutsaert, W., 2005. Hydrology. An introduction. Cambridge University Press, Cambridge, UK.

Cowan, I., 1972. Oscillations in stomatal conductance and plant functioning associated with stomatal conductance: Observations and a model. Planta 106 (3), 185–219.

Dingman, S., 2002. Physical hydrology. Prentice Hall, New Jersey.

Eagleson, P., 2002. Ecohydrology. Darwinian expression of vegetation form and function. Cambridge University Press.

Farahani, H., Howell, T., Shuttleworth, W., Bausch, W., 2007. Evapotranspiration: Progress in measurement and modeling in agriculture. Transactions of the ASABE 50 (5), 1627–1638.

Gates, D., 1960. Biophysical Ecology. Springer-Verlag, New York.

Gates, D., Alderfer, R., Taylor, S., 1968. Leaf temperature of desert plants. Science 159, 994–995.

Hall, W., 1971. Biological hydrological systems. In: Proceedings of the 3rd Internantional Seminar for Hydrology Professors. Purdue University, West Lafayette, Ind., pp. 1–7.

Harvey, G., 1979. Photosynthetic performance of isolated leaf cells from sun and shade plants. Year Book - Carnegie Institution of Washington (79), 161–164.

Hubbard, R., Bond, B., Ryan, M., 1999. Evidence that hydraulic conductance limits photosynthesis in old Pinus ponderosa trees. Tree Physiology 19, 165–172.

Kramer, P., Kozlowsku, T., 1960. Physiology of trees. McGraw-Hill, New York.

Kustas, W., Rango, A., Uijlenhoet, R., 1994. A simple energy budget algorithm for the snowmelt runoff model. Water Resources Research 30, 1515–1527.

Lafleur, P., Roulet, N., 1992. A comparison of evaporation rates from two fens of the Hudson Bay lowland. Aquat. Bot. 44, 59–69.

Lang, A., Klepper, B., Cumming, M., 1969. Leaf Water Balance During Os-

cillation of Stomatal Aperture. Plant Physiology 44 (6), 826.
Larcher, W., 1983a. Physiological Plant Ecology, 2nd Edition. Springer-Verlag, Berlin.
Larcher, W., 1983b. Physiological Plant Ecology, 2nd Edition. Springer-Verlag, Berlin, p. 27.
Larcher, W., 1997. Physiological Plant Ecology: Ecophysiology and Stress Physiology of Functional Groups, 3rd Edition. Springer-Verlag.
Lavigne et al., M., 1997. Comparing nocturnal eddy covariance measurements to estimates of ecosystem respiration made by scaling chamber measurements at six coniferous boreal sites. J. Geophys. Res. 102, 28977–29985.
Law, B., Goldstein, A., Anthoni, P., Unsworth, M., Panek, J., Bauer, M., Fracheboud, J., Hultman, N., 2001. co_2 and water vapor exchange by young and old ponderosa pine ecosystem during a drough year. Tree Physiol. 21, 299–308.
Mahrt, L., 1999. Stratified atmospheric boundary layers. Boundary Layer Meteorology 90, 375–396.
Monteith, J., 1965. Evaporation and the environment. Symp. Soc. Exper. Biol. 19, 205–234.
Monteith, J., 1973. Principles of Environmental Physics. Elsevier, New York, p. 183.
Peart, R., Curry, R. (Eds.), 1998. Agricultural systems modeling and simulation. Marcel Deker, Inc., New York, NY, Ch. 7, pp. 200–210.
Phillips, N., Bond, B., McDowell, N., Ryan, M., 2002. Canopy and hydraulic conductance in young, mature and old Douglas-fir trees. Tree Physiology 22 (2/3), 205–212.
Pothier, D., Margolis, H., Waring, R., 1989. Patterns of change of saturated sapwood permeability and sapwood conductance with stand development. Canadian journal of forest research 19 (4), 432–439.
Reid, D., Silins, U., Mendoza, C., Lieffers, V., 2005. A unified nomenclature for quantification and description of water conducting properties of sapwood xylem based on Darcy's law. Tree Physiology 25 (8), 993–1000.
Rijtema, P., 1965. An analysis of actual evapotranspiration. Report 659, Centre Agric. Publ. Agricultural Research.
Shuttleworth, W. J., 2006. Towards One-Step Estimation of Crop Water Requirements. Trans. of the ASABE 49 (4), 925–935.
Sperry, J., 2000. Hydraulic constraints on plant gas exchange. Agricultural and Forest Meteorology 104 (1), 13–23.
Steudle, E., 1995. Trees under tension. Nature 378 (6558), 663–664.
Taiz, L., Zeiger, E., 2002. An introduction to solar radiation, 3rd Edition. Sinauer Associates, Inc., Sunderland , Massachusetts.
Thom, A., 1972. Momentum, mass, and heat exchange of vegetation. Quart. J. Roy. Meteorol. Soc. 98, 124–134.
Tuzet, A., Perrier, A., Leuning, R., 2003. A coupled model of stomatal conductance, photosynthesis and transpiration. Plant, Cell & Environment 26 (7), 1097–1116.

Tyree, M., 2003. The ascent of water. Nature 423, 923.
Verma, S., Baldocchi, D., Anderson, D., Matt, D., Clement, R., 1986. Eddy fluxes of co_2, water vapour, and sensible heat over a decidous forest. Boundary-Layer Meteorology 36, 71–91.
Wang, J., Bras, R., Lerdau, M., Salvucci, G., 2007. A maximum hypothesis of transpiration. Journal of Geophysical Research 112, G03010.
Wang, J., Salvucci, G., Bras, R., 2004. An extremum principle of evaporation. Water Ressources Research 40, W09303.
Wilson et al., K., 2002. Energy balance closure at fluxnet sites. Agricultural and Forest Meteorology 113, 223–243.
Witkowski, E., Lamont, B., 1991. Leaf specific mass confounds leaf density and thickness. Oecologia 88, 486–493.

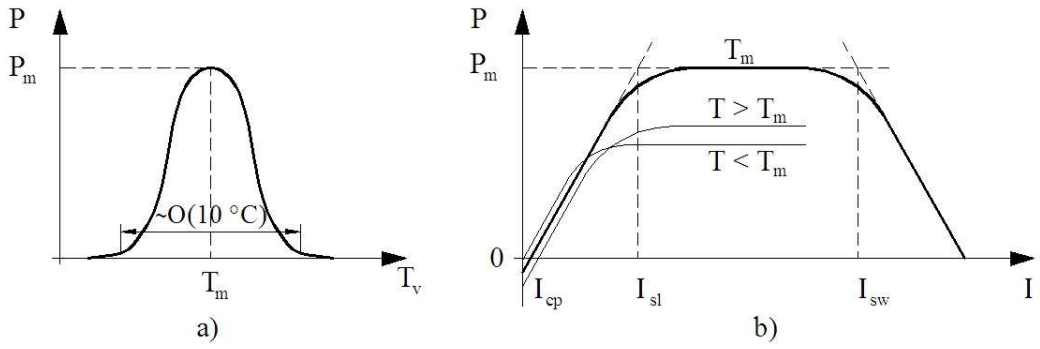

Fig. 1. Net photosynthesis as a function of leaf temperature (a) and insolation level (b) for different leaf temperatures (adapted from Eagleson (2002), fig. 8.2)

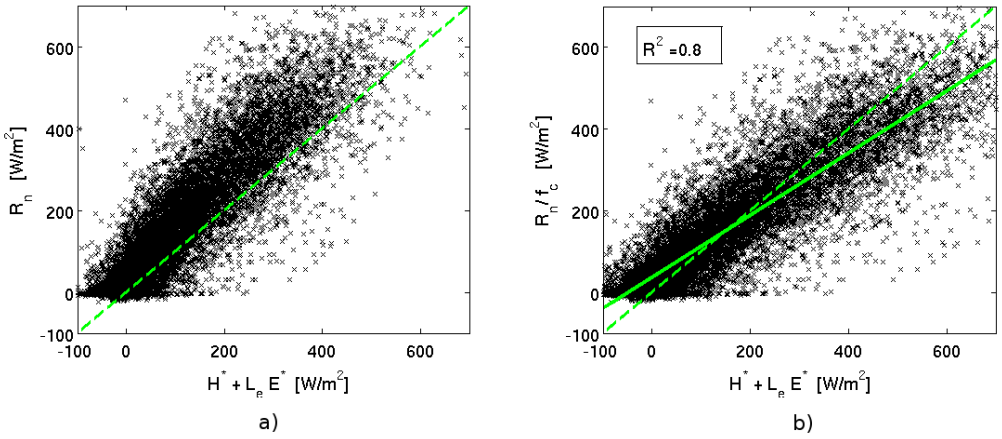

Fig. 2. The measured (a) and the corrected (b) net radiation input versus the measured surface fluxes for site no. 15 (dashed line - 1:1 line; solid line - the linear regression line)

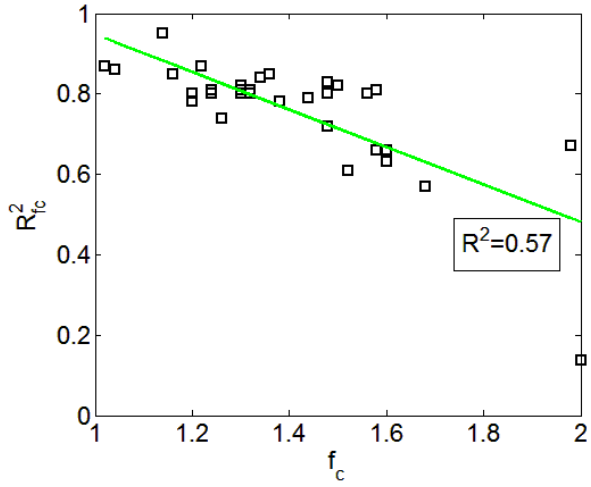

Fig. 3. The correction factor f_c with respect to the correlation coefficient R^2_{fc}

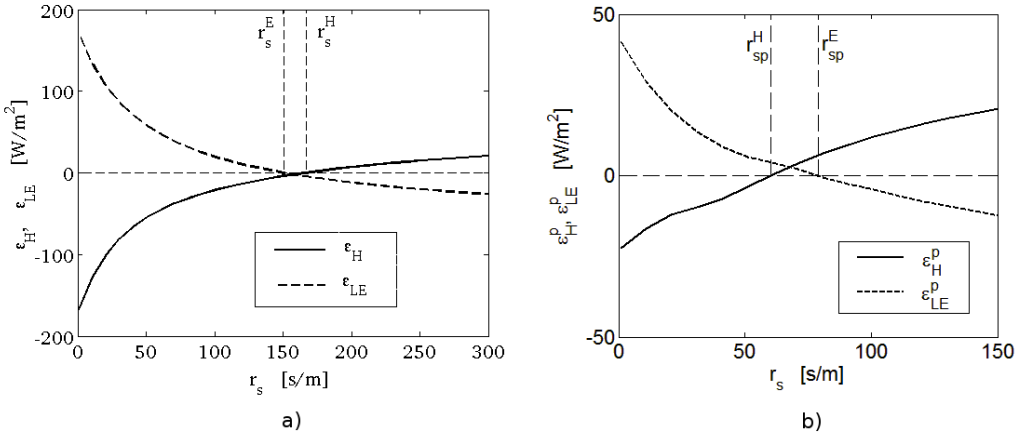

Fig. 4. The mean errors between computed and measured surface fluxes as a function of r_s for site no. 15: (a) error averaged over the period of study defined in section 4; (b) error averaged over the selected humid period defined in section 4.4

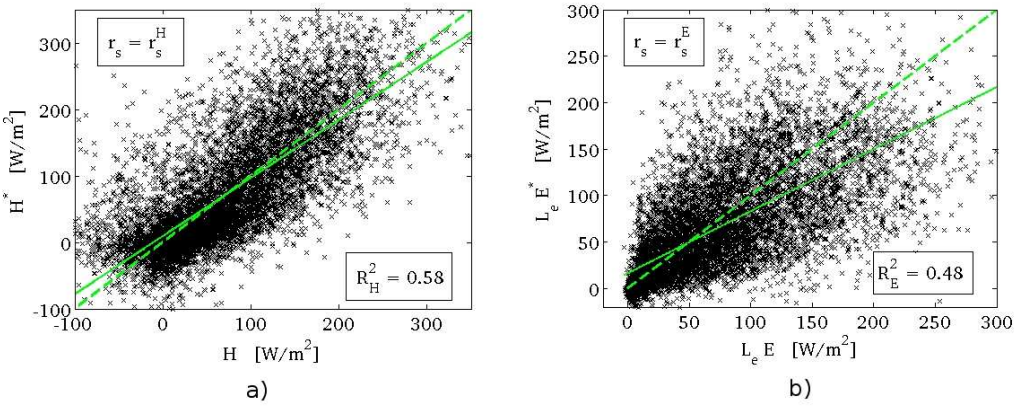

Fig. 5. The modeled sensible heat flux (H) versus the actual sensible heat flux (H^*) (a) and the modeled latent heat flux (L_eE) versus the actual latent heat flux (L_eE^*) (b) for site no. 15 (dashed line - 1:1 line; solid line - the linear regression line)

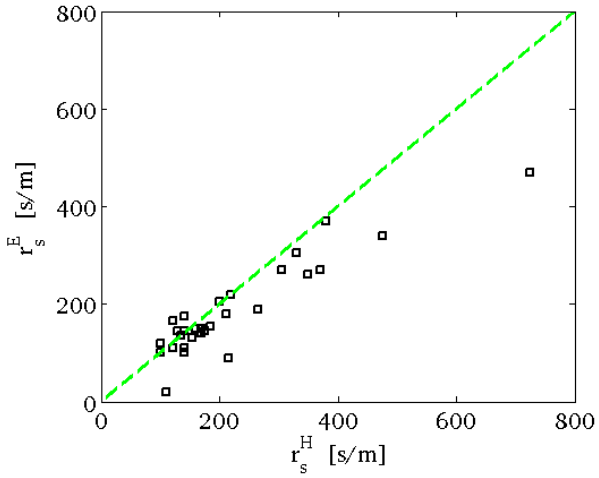

Fig. 6. r_s^H versus r_s^E for all sites in Table 1

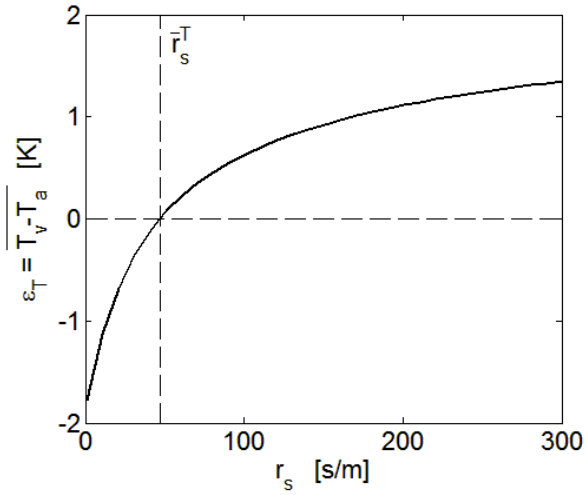

Fig. 7. The mean error between vegetation and air temperatures, ϵ_T, for site no. 15 and as a function of r_s (the error is averaged over the period of study defined in section 4)

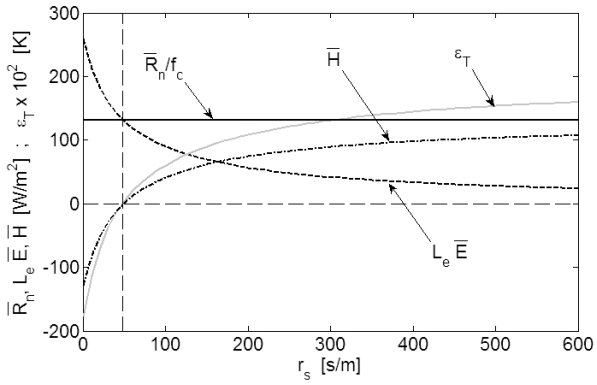

Fig. 8. The averaged latent and sensile heat fluxes and ϵ_T with respect to r_s for site no. 15 (the average is made over the study period defined in section 4)

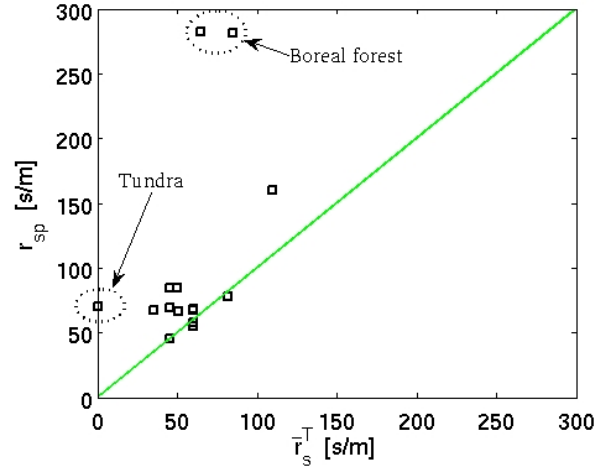

Fig. 9. $\overline{r}_s^T$ versus $\overline{r}_{sp}$

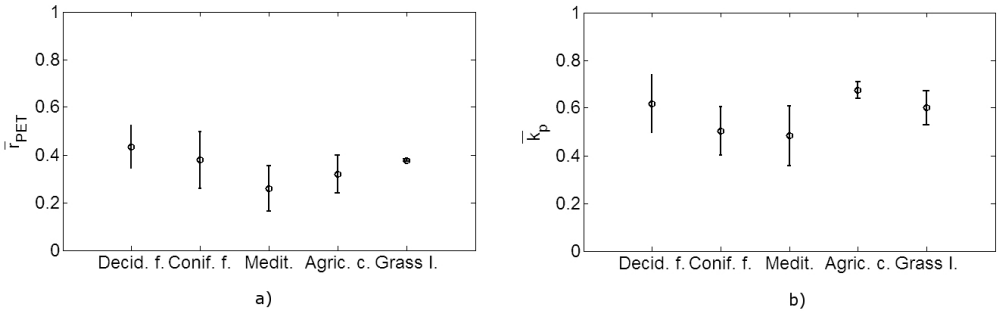

Fig. 10. a) The variation of $\overline{r}_{PET}$ with respect to each biome; b) The variation of $\overline{k}_p$ with respect to each biome

Table 1
The analyzed FLUXNET stations

No.	Site Name	Location	Lat/Long	Period
Deciduous forest				
1	Harvard forest (HV)	MA/USA	$42^o32'N/72^o11'W$	1992-1999
2	WalkerBranch (WB)	TN/USA	$35^o58'N/84^o17'W$	1995-1998
3	Hesse forest(HE)	France	$48^o40'N/7^o04'E$	1996-1999
4	Gunnarsholt (GU)	Iceland	$63^o50'N/23^o13'W$	1996-1998
5	Park Falls (WL)	WI/USA	$45^o56'N/90^o16'W$	1997-1999
6	Soroe (SO)	Denmark	$55^o29'N/11^o38'E$	1996-1999
7	Manaus (MA)	Brazil	$2^o36'S/60^o12'W$	1996
8	Willow Creek (WC)	WI/USA	$45^o48'N/90^o04'W$	1999
Evergreen forest				
9	Braaschaat (BR)	Belgium	$51^o18'N/4^o31'E$	1996-1998
10	Loobos (LO)	Netherlands	$52^o10'N/5^o44'E$	1996-1998
11	Sask (JP)	Canada	$53^o54'N/104^o39'W$	1994
12	Wind River Crane (WR)	WA/USA	$45^o49'N/121^o57'W$	1998
13	Tharandt (TH)	Germany	$50^o57'N/13^o34'E$	1996-1999
14	Norunda (NO)	Sweden	$60^o05'N/17^o29'E$	1996-1998
15	Flakaliden (FL)	Sweden	$64^o06'N/19^o27'E$	1996-1998
16	Bayreuth (WE)	Germany	$50^o08'N/11^o52'E$	1996-1998
17	Hyytiala (HY)	Finland	$61^o50'N/24^o17'E$	1996-1998
18	Howland forest (HL)	ME/USA	$45^o12'N/68^o44'W$	1996-1997
19	Duke forest (DU)	NC/USA	$35^o58'N/79^o05'W$	1998-1999
20	Boreas NSA (NB)	Canada	$55^o52'N/98^o28'W$	1994-1998
21	Griffin, Aberfeldy (AB)	UK	$56^o36'N/3^o47'W$	1997-1998
22	Niowt Ridge forest (NW)	CO/USA	$40^o01'N/105^o32'W$	1999
Evergreen Mediterranean climate				
23	Blodgett forest (BL)	CA/USA	$38^o53'N/120^o37'W$	1997-2000
24	Metolius (ME)	OR/USA	$44^o29'N/121^o37'W$	1996-1997
25	Castelporziano (CP)	Italy	$41^o42'N/12^o22'E$	1997-1998
Agricultural crops				
26	Bondville (BV)	IL/USA	$40^o00'N/88^o17'W$	1997-1999
27	Ponca City (PO)	OK/USA	$36^o46'N/97^o08'W$	1997
Grasslands				
28	Little Washita (LW)	OK/USA	$34^o57'N/97^o58'W$	1996-1998
29	Shidler (SH)	OK/USA	$36^o56'N/96^o41'W$	1997
Tundra				
30	Happy Valley (HA)	AK/USA	$68^o08'N/148^o50'W$	1994-1995
31	Atqasuk (AT)	AK/USA	$70^o28'N/157^o24'W$	1999
32	Barrow (BA)	AK/USA	$71^o19'N/156^o37'W$	1998-1999

Table 2
Results

No.	f_c	R^2_{fc}	r^H_s	r^E_s	$R^2_H (R^2_E)$	$\overline{r}^T_s$	k_p	R^2_{PET}	r^H_{sp}	r^E_{sp}
	–	–	s/m	s/m	–	s/m	–	–	s/m	s/m
Deciduous temperate forest										
1 [1]	1.24	0.81	121	111	0.56 (0.54)	41	0.60	0.53	–	–
2	1.44	0.79	135	135	0.41 (0.51)	60	0.75	0.52	71	65
3	1.58	0.81	101	101	0.62 (0.53)	51	0.70	0.57	61	71
4	1.48	0.83	121	165	0.60 (0.60)	41	0.50	0.58	40	150
5 [2 3]	1.52	0.61	141	110	0.20 (0.24)	82	1	0.24	85	70
6 [2]	1.32	0.80	160	150	0.58 (0.42)	50	0.45	0.48	75	95
7 [1]	1.38	0.78	140	145	0.57 (0.66)	45	0.70	0.71	–	–
8 [3]	2.00	0.14	215	90	0.01 (0.44)	65	1.1	0.43	140	60
	1.42	**0.78**	**131.3**	**131**	**0.51 (0.5)**	**52.9**	**0.67**	**0.52**	**66.4**	**90.2**
Evergreen temperate forest										
9 [3]	1.68	0.57	170	150	0.31 (0.23)	60	0.60	0.26	35	75
10	1.3	0.80	100	120	0.33 (0.45)	45	0.50	0.45	8	75
11 [1]	1.20	0.80	305	270	0.70 (0.10)	75	0.45	0.10	–	–
12 [1 3]	1.98	0.67	725	470	0.57 (0.07)	120	0.45	0.10	–	–
13	1.32	0.81	170	140	0.61 (0.34)	60	0.55	0.37	60	55
14	1.24	0.80	170	150	0.50 (0.35)	60	0.55	0.38	60	75
15	1.48	0.80	166	150	0.58 (0.48)	47	0.50	0.49	60	78
16	1.50	0.82	200	205	0.64 (0.47)	50	0.40	0.51	35	105
17 [3]	1.60	0.66	130	145	0.23 (0.71)	45	0.55	0.75	30	130
18 [4]	1.34	0.84	–	–	–	–	–	–	–	–
19 [1]	1.56	0.80	220	220	0.48 (0.43)	100	0.65	0.43	–	–
20	1.30	0.82	370	270	0.81 (0.35)	85	0.40	0.45	277	285
21	1.36	0.85	330	305	0.87 (0.18)	65	0.30	0.21	265	300
22	1.26	0.74	140	100	0.69 (0.29)	35	0.60	0.29	200	30
	1.39	**0.78**	**206.3**	**185.4**	**0.56 (0.37)**	**60.4**	**0.50**	**0.39**	**103**	**120.8**
									59.8 [5]	**70.9** [5]
Mediterranean climate										
23	1.20	0.78	212	180	0.64 (0.52)	60	0.60	0.54	50	60
24 [3]	1.60	0.63	475	340	0.55 (0.14)	90	0.50	0.20	90	55
25 [1]	1.48	0.72	350	260	0.64 (0.33)	35	0.35	0.44	–	–
	1.43	**0.71**	**345.7**	**260**	**0.61 (0.33)**	**61.7**	**0.48**	**0.39**	**70**	**57.5**
Agricultural crops										
26	1.16	0.85	175	145	0.27 (0.57)	35	0.70	0.53	75	60
27	1.04	0.86	265	190	0.21 (0.37)	45	0.65	0.40	25	65
	1.10	**0.86**	**220**	**167.5**	**0.24 (0.47)**	**40**	**0.68**	**0.47**	**50**	**62.5**
Grasslands										
28	1.22	0.87	380	370	0.33 (0.32)	110	0.55	0.35	150	170
29	1.30	0.81	140	175	0.85 (0.51)	45	0.65	0.53	55	115
	1.26	**0.84**	**260**	**272.5**	**0.59 (0.42)**	**77.5**	**0.60**	**0.44**	**102.5**	**142.5**
Tundra										
30	1.02	0.87	185	155	0.66 (0.65)	0	0.60	0.68	65	75
31	1.14	0.95	155	130	0.84 (0.81)	0	0.55	0.86	50	90
32 [3]	1.58	0.66	110	20	0.64 (0.52)	0	0.80	0.52	300	0
	1.25	**0.83**	**150**	**101.7**	**0.71 (0.66)**	**0**	**0.65**	**0.69**	**138.3**	**55**

[1] Absent/sparse precipitation data
[2] Net radiation is not available
[3] Energy balance closure is very weak
[4] Wind speed data is absent
[5] Sites no. 20 and 21 are excluded from this average